PERGAMON

International Journal of Heat and Mass Transfer 43 (2000) 39–51

International Journal of HEAT and MASS TRANSFER

www.elsevier.com/locate/ijhmt

Effect of fin spacing on convection in a plate fin and tube heat exchanger

Ricardo Romero-Méndez, Mihir Sen*, K.T. Yang, Rodney McClain

Department of Aerospace and Mechanical Engineering, University of Notre Dame, Notre Dame, IN 46556, USA

Received 26 May 1998; received in revised form 2 April 1999

Abstract

We examine the influence of fin spacing on the over-tube side of a single-row fin-tube heat exchanger through flow visualization and numerical computation. The distance between fins is nondimensionalized by the tube diameter. If this parameter is small, the flow is Hele-Shaw; as it is increased, a horseshoe vortex is formed just upstream of the tube; a separated region is then developed behind the tube; this becomes larger and eventually communicates with the fluid downstream of the heat exchanger. A peak in the Nusselt number occurs at the horseshoe vortex. In the wake region the Nusselt number is very small but increases when there is fluid exchange with that downstream. The ratio of the overall Nusselt number per unit length to the nondimensional pressure drop is found to show a maximum.

1. Introduction

The plate-fin and tube geometry is a common configuration in heat exchangers. In this paper we will restrict our study to a single-row heat exchanger where the flow is over a series of transverse tubes and the fins are flat. These heat exchangers are commonly operated with liquid inside the tubes and air on the outside, because of which the external thermal resistance is usually the most critical. Our objective here is to determine the influence of the distance between fins on the convection of heat.

Some of the characteristics of the hydrodynamics of plate-fin and tube geometries are: boundary layers developing from the leading edges of the fins and over the tube, roll-up of these boundary layers into horseshoe vortices ahead and around the tube, separation of the boundary layer on the tube and recirculation bubbles or vortex shedding in the wake. At small fin spacings the streamlines are analogous to those for potential flow over a cylinder [1]. At the other extreme of infinite fin spacing, the flow is that around a cylinder [2]. The flow at a single cylinder-plate junction has also been analyzed in some detail by Baker [3,4] and others. The plate-fin and tube heat exchanger geometry corresponds to a cylinder of finite length bounded by two plates so that the flow at each cylinder-plate junction may interfere with the other. The hydrodynamics of this problem has been studied by Bossel and Honnold [5] who used dye visualization in a low-speed water tunnel. Multiple horseshoe vortices were observed for the experiments at the higher Reynolds numbers.

The heat transfer problem is strongly related to the hydrodynamics. The experiments of Saboya and Sparrow [6], using a mass transfer analogy, correspond to heat transfer from isothermal fins; they showed that the transfer rate is high on the forward part of the fins due to developing boundary layers as well as in front

* Corresponding author. Tel.: +1-219-631-5975; fax: +1-219-631-8341.

E-mail address: mihir.sen.1@nd.edu (M. Sen)

0017-9310/00/$ - see front matter
PII: S0017-9310(99)00120-9

Nomenclature

A_f	fin surface area	Re_s	Reynolds number based on distance between fins
d	tube diameter	Re^*	reduced Reynolds number
l_c	distance of tube center from leading edge	Re_{ext}	Reynolds number based on V_{ext}
L_c	$=l_c/d$	s	distance between fins
l_f	fin length	S	$=s/d$
L_f	$=l_f/d$	T	nondimensional fluid temperature
l_{x_1}	length of computational domain ahead of fins	T^*	dimensional fluid temperature
L_{x_1}	$=l_{x_1}/d$	T^*_w	dimensional wall temperature
l_{x_2}	length of computational domain after fins	T^*_{in}	dimensional fluid temperature at entrance
L_{x_2}	$=l_{x_2}/d$	$\bar{T}_{exit}$	mean exit temperature
Nu	local Nusselt number	$\mathbf{u}$	nondimensional velocity vector
$\overline{Nu}$	overall Nusselt number	V	mean velocity of fluid between fins
p	nondimensional pressure	V_{ext}	velocity of water in tunnel
Δp	nondimensional pressure drop	w	pitch
Pr	Prandtl number	W	$=w/d$
Re	Reynolds number based on tube diameter	x, y, z	nondimensional Cartesian coordinates
		ρ	fluid density

of the tube due to a vortex system there. This was confirmed by Ireland and Jones [7] who made heat transfer measurements using a transient method based on thermochromic liquid crystals. The Nusselt number on the cylinder surface was found to be the least near the wall.

Numerical methods have also been used for this problem. Haught and Engelmann [8] used a finite element method and reported examples of velocity and temperature fields. Torikoshi et al. [9] modeled the plate-fin and tube heat exchanger located in a uniform field using a three-dimensional unsteady numerical computation and reported good agreement with experimental data. In a series of papers, Fiebig and coworkers [10–12] used numerical methods to understand the flow and convection in a fin-tube geometry as well as heat transfer augmentation by vortex generators. In Fiebig et al. [11] they report on the results of finite-volume calculations of the flow and conjugate heat transfer in a fin-tube geometry. They investigated the flow patterns, pressure distribution, Nusselt number distribution, and fin efficiency, all as a function of Reynolds number but with a fixed geometry. An interesting region of heat transfer reversal was found in the

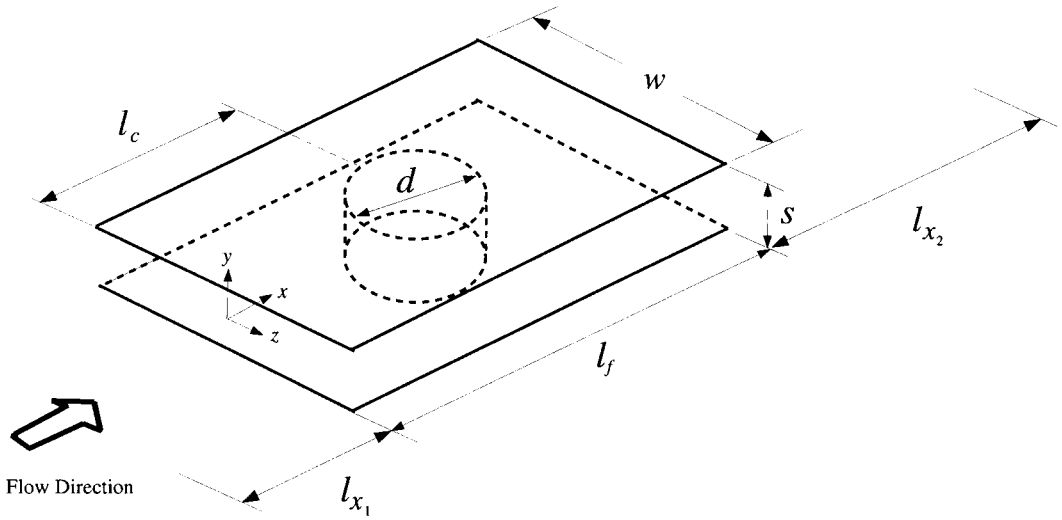

Fig. 1. Region of flow analysis.

wake due to the finite fin conductivity. Jang et al. [13] show the results of a numerical study in which the overall Nusselt number and pressure drop are shown as a function of the fin-spacing based Reynolds number.

There are many factors that have an effect on the heat transfer from the heat exchanger as well as on the pressure drop across it. Previous investigations have determined the influence of the flow Reynolds number and the fin efficiency. The effect of geometrical parameters on the operation of the fin-tube heat exchanger has so far not been analyzed. One of the most important is the distance between fins which plays an important role in the optimization of heat exchanger design. The effect of fin spacing is what we will study here; either too many or too few fins per unit length can be expected to have an adverse effect on the performance of a heat exchanger, so that an optimum fin spacing can reasonably be expected.

2. Problem description

Our objective is to understand the hydrodynamics of the flow and the corresponding heat transfer as a function of the fin spacing, keeping the other parameters constant. To combine the advantages of both experimental and computational techniques, we will use flow visualization as well as numerical calculation of the velocity and temperature fields. Heat transfer experiments are not carried out here because of the difference in the Prandtl number between the water in the water-tunnel used and the air in which the heat exchanger will operate. Experimental and numerical details not given here are in Romero-Méndez [14].

The fin-tube geometry is shown in Fig. 1. The important lengths are d, s, w, l_c and l_f which are the tube diameter, the distance between fins, the pitch of the tubes, the tube location and the fin length, respectively. Taking a specific commercial heat exchanger as a

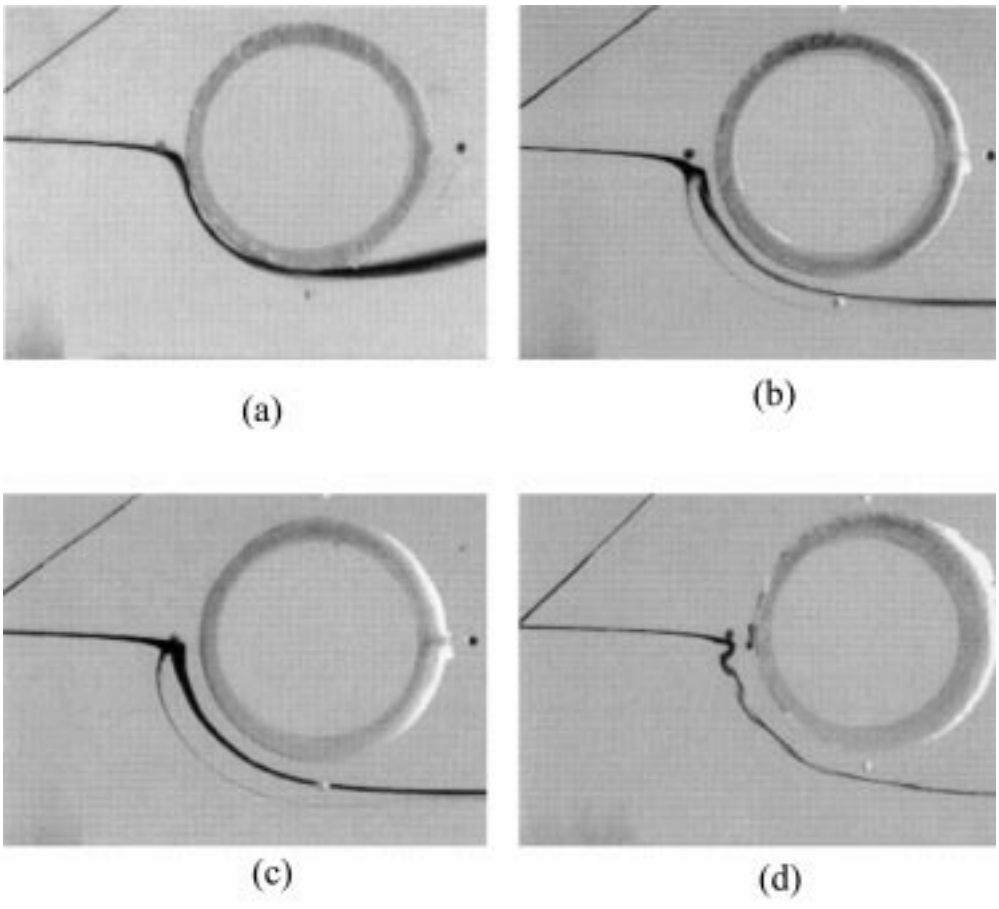

Fig. 2. Horseshoe vortex visualization for varying fin spacing. Flow is from left to right. (a) $S = 0.116$, $Re = 1200$, (b) $S = 0.190$, $Re = 1310$, (c) $S = 0.265$, $Re = 1430$, (d) $S = 0.365$, $Re = 1460$.

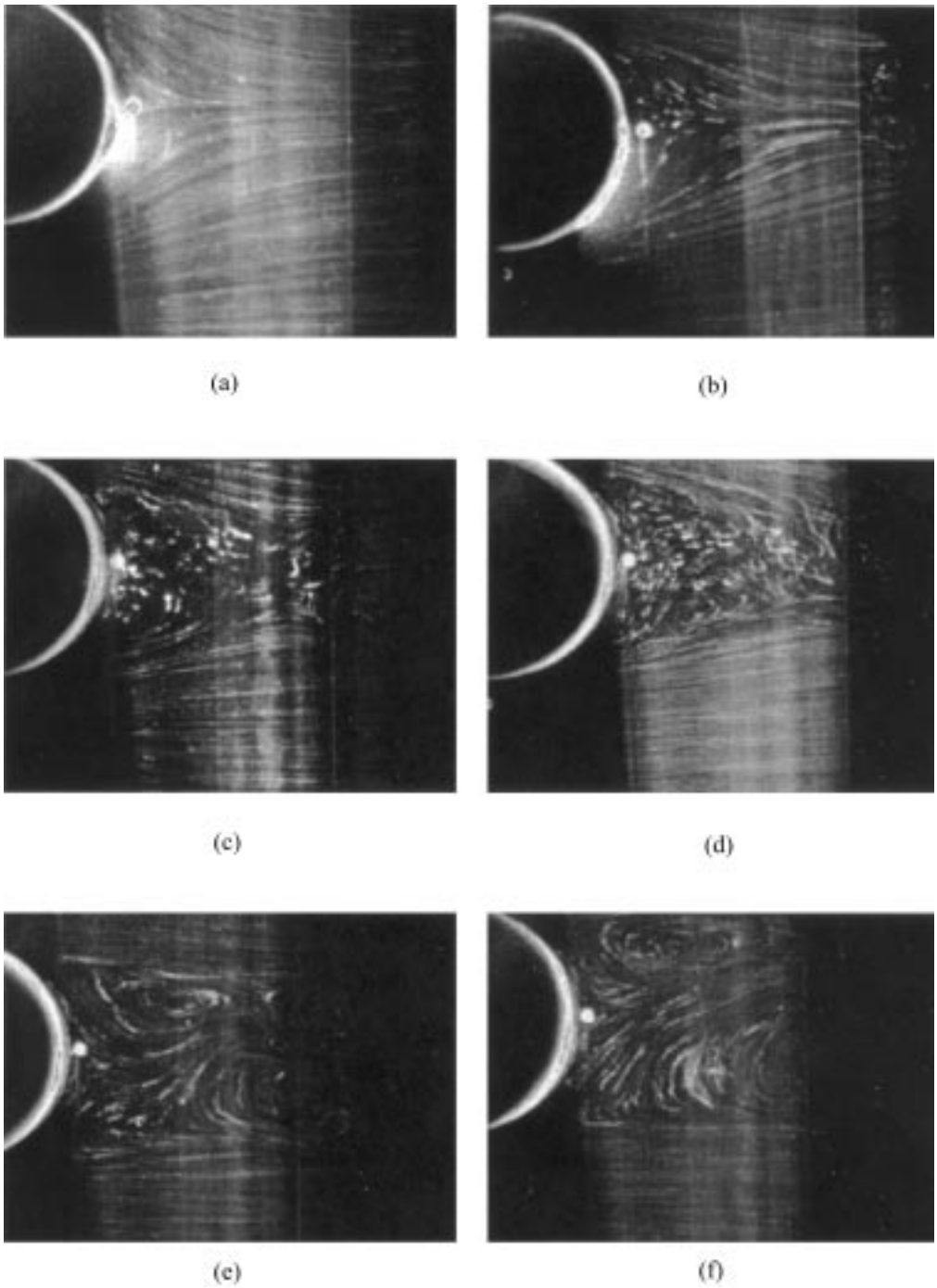

Fig. 3. Wake flow visualization for varying fin spacing. Flow is left to right. (a) $S = 0.116$, $Re = 260$, (b) $s = 0.165$, $Re = 360$, (c) $S = 0.190$, $Re = 380$, (d) $S = 0.215$, $Re = 390$, (e) $S = 0.265$, $Re = 420$, (f) $S = 0.365$, $Re = 480$.

model, the experiments will be in a scaled-up version of that geometry, while for the computations the nondimensional parameters, $S=s/d$, $W=w/d$, $L_c=l_c/d$, $L_f=l_f/d$, will be kept similar to those in the model. The commercial heat exchanger model comes with fin spacings in the $0.128 \leq S \leq 0.240$ range.

We will define the Reynolds number, Re, based on the mean velocity of the flow between the plates and the tube diameter; with this choice we can vary the nondimensional distance between fins and the Reynolds number independently of each other. Other characteristic lengths could have been used to define the Reynolds number; for the distance between fins as the characteristic length, we get $Re_s=SRe$; the reduced Reynolds number defined as $Re^*=S^2Re$ is appropriate for the Hele-Shaw limit [15].

3. Flow visualization

The test model consists of three PVC tubes held between two Plexiglas plates. Different distances between fins are obtained using tubes of different lengths. The region of interest in the experiment is the space between the plates and around the central tube, the other two providing symmetry conditions. The tubes are cylindrical slices of short length that do not protrude to the exterior of the plates to avoid disturbances from the exterior affecting the flow downstream. The model was suspended in a water tunnel, an Eidetics International Model 1520, which has a working section that is 0.381 m wide, 0.508 m deep, and 1.626 m long. Practical and sustainable flow speeds were in the 0.0915–0.1525 m/s range.

Several techniques were used for visualization. For the wake region the water tunnel was seeded with 14 μm diameter silver-coated hollow glass spheres manufactured by Potters Inc. and the flow was illuminated by an 30 mW He–Ne laser light to produce a slice of the flow field. The rest of the flow ahead and around the tube was visualized using diluted food coloring dye injected normal to the plates at the leading edge of one of them.

The water tunnel speed, V_{ext}, could be controlled through a water pump. This speed is, however, different from the average speed of the flow between the plates, V, due to the different resistances to the flow inside and outside the plates. This difference becomes more accentuated as the fin spacing is reduced. Since it was difficult to keep V constant, in the experiments we varied the fin spacing but kept V_{ext} and its corresponding Reynolds number Re_{ext} constant. For each V_{ext} and s, V was measured at the entrance by producing hydrogen bubbles from a wire in the midplane between the fins, illuminating them by a 30 mW He–Ne laser lamp, and tracking them with a video camera. An uncertainty analysis of the velocity measurement shows an error of $\pm 6.6\%$.

Dye visualization of the horseshoe vortex was performed for $Re_{ext} \geq 630$; its use at smaller Reynolds numbers proved to be difficult because of dye oscillations and diffusion. The horseshoe vortex system was made visible with this technique, and observations showed no vortex, one vortex, or two vortices depending on the fin spacing and Reynolds number. Fig. 2(a)–(d) show the effect that the fin spacing has on the horseshoe vortex system. It cannot be detected at the smaller fin spacing in Fig. 2(a) but is clearly visible in Fig. 2(d). For the larger fin spacings the vortex tubes also become larger and displace themselves away the tube.

Visualization of the wake was through 16 s exposure pictures of the streaklines corresponding to the seeded particles. The influence of fin spacing is shown in Fig. 3(a)–(f). For small fin spacings, as in Fig. 3(a), the flow around the tube does not separate and it resembles the Hele-Shaw limit. As the fin spacing is increased, it separates and there is a closed recirculation bubble as seen in Fig. 3(b). The width of the wake region increases until it covers the entire back side of the tube. On further increasing the fin spacing, the recirculation region begins to communicate with the flow downstream of the heat exchanger and there is even a reverse, reentrant flow towards the tube which can be observed in Fig. 3(c). For small fin spacings the wake is steady as Fig. 3(a)–(c) show, and is unsteady for larger spacings as in Fig. 3(d)–(f). That the reentrant flow brings back the unsteadiness that may be present downstream was confirmed by artificially increasing it. This unsteadiness in the wake of the heat exchanger is dependent on the relative fin thickness which is larger than normal in this experiment.

There is good agreement between the experimental and the steady-state numerical results below as far as the shape of the recirculation zone is concerned. Comparison is not possible, however, when the wake becomes unsteady since the numerical method becomes inapplicable.

4. Numerical analysis

The flow in Fig. 1 is in the x direction. In nondimensional terms, the heat exchanger itself is in $0 \leq x \leq L_f$ and the computational domain is defined by $-L_{x_1} \leq x \leq L_f + L_{x_2}$, $0 \leq y \leq S/2$, $0 \leq z \leq W/2$ and $(x-L_c)^2 + y^2 \geq 0.25$. The computational domain extends farther than the heat exchanger both upstream and downstream of it for more accurate application of the boundary conditions and to reduce numerical oscillations. The nondimensional geometrical parameters

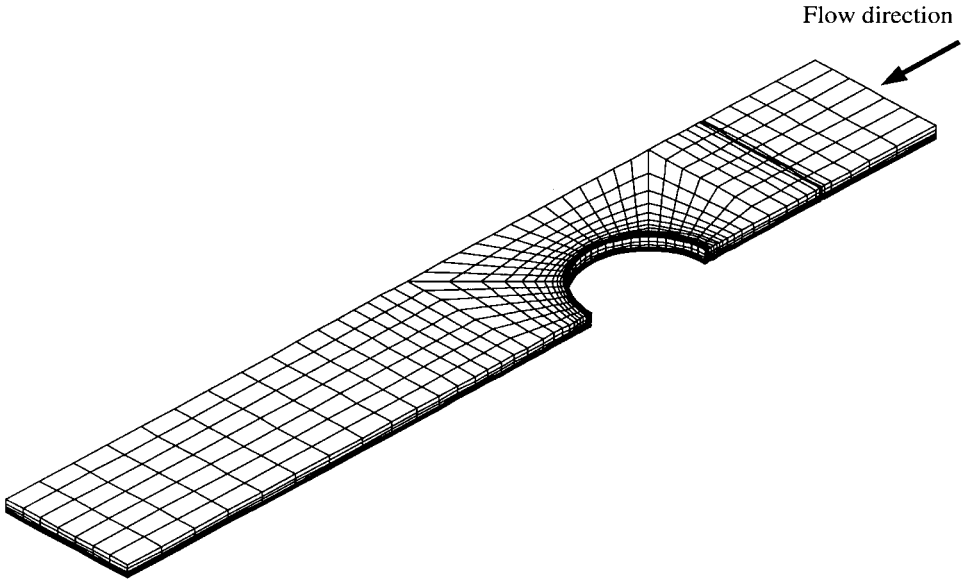

Fig. 4. Typical mesh of computational domain.

used for the computation are $W = 1.0625$, $L_f = 3.1$, $L_c = 1.525$, $L_{x_1} = l_{x_1}/d = 1$, $L_{x_2} = l_{x_2}/d = 3.1$.

The flow is assumed to be steady, Newtonian, incompressible and laminar. The characteristic values for nondimensionalization are: velocity V, length d, pressure ρV^2, where ρ is the fluid density. The temperature, T^*, is nondimensionalized by $T = (T^* - T^*_{in})/(T^*_w - T^*_{in})$, where T^*_{in} is the fluid inlet temperature and T^*_w is the wall temperature, both assumed constant. Assumption of an isothermal fin and tube surface, which is valid for large thermal conductivity of the fin material or a large fin thickness, is equivalent to a fin efficiency of unity; the influence of more realistic fin conditions was studied by Fiebig et al. [11]. The governing nondimensional continuity, momentum and energy equations are

$$\nabla \dot{\mathbf{u}} = 0 \tag{1}$$

$$(\dot{\mathbf{u}} \nabla)\mathbf{u} = -\nabla p + \frac{1}{Re}\nabla^2 \mathbf{u} \tag{2}$$

$$(\dot{\mathbf{u}} \nabla)T = \frac{1}{RePr}\nabla^2 T \tag{3}$$

where $\mathbf{u}$ is the velocity vector, p is the pressure, and Pr is the Prandtl number (taken to be 0.72 here). The boundary conditions are no-slip and constant temperature at the solid walls, velocity and temperature symmetry at the $y = 0$ and $z = 0$ planes, uniform velocity and temperature at the entrance section, and zero normal derivatives at the outflow and at the $z = W/2$ sections. The convective heat transfer distribution on the fin and tube surface is represented by the local Nusselt number, Nu, which is equal to the normal component of the nondimensional temperature gradient at any point. This definition is different from that of Fiebig et al. [11] and Jang et al. [13] who use the bulk temperature at a given section for reference.

A general-purpose program for fluid mechanics and heat transfer, FIDAP,[1] is used to solve the problem. The numerical technique is based on the finite element method which has the advantages of being flexible in its ability to adapt to complex geometries, permitting a distribution of grid density, and easy specification of boundary conditions on curved surfaces. The three-dimensional finite element mesh used is shown in Fig. 4. Eight node brick elements with linear interpolation were used to mesh the domain. The velocity degrees of freedom are at each node while the pressure degree of freedom is associated with the element centroid.

The following were some of the settings used in the actual implementation of the code:

- PRESSURE PENALTY: the penalty parameter was set at 10^{-7}. This value is small enough to approximate incompressibility well yet large enough to prevent the resulting matrix from being too ill-conditioned.
- The nonlinear system of algebraic equations was solved in a simultaneous, coupled manner because of the quick convergence attained even though the

[1] From Fluent Incorporated, Lebanon, NH, USA.

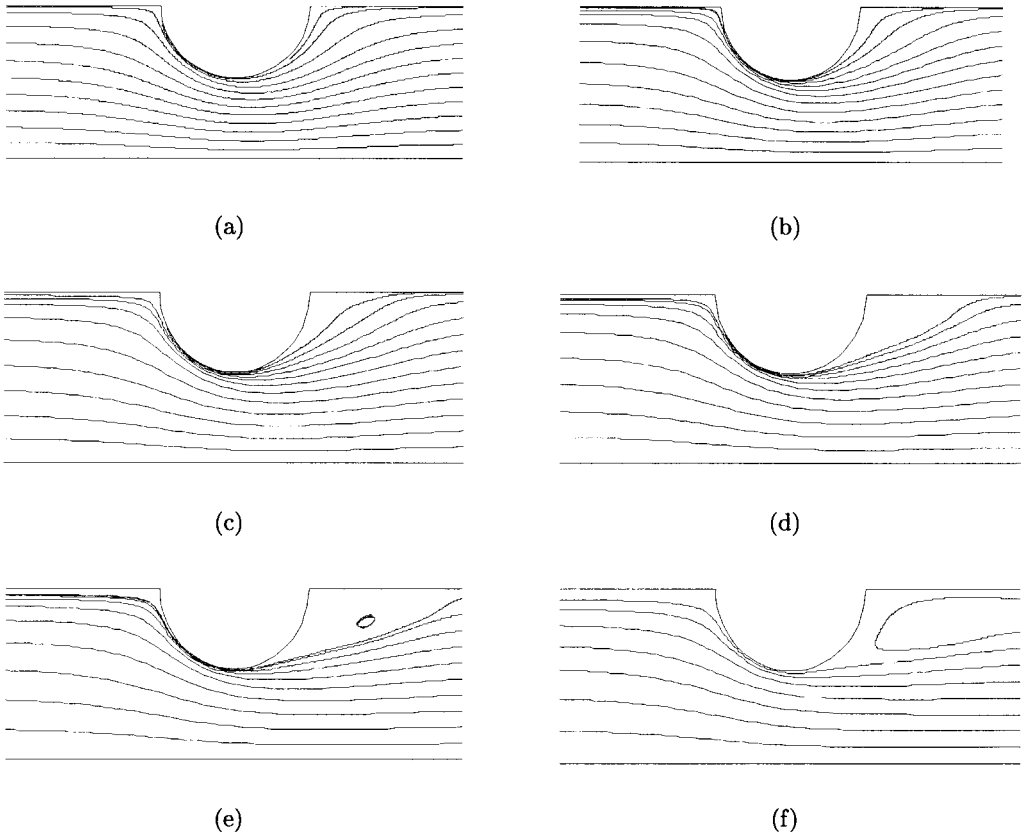

Fig. 5. Numerical visualization of pathlines on plane $y = 0$ for varying fin spacing, and $Re = 260$. Flow is from left and right. (a) $S = 0.116$, (b) $S = 0.165$, (c) $S = 0.190$, (d) $S = 0.215$, (e) $S = 0.265$, (f) $S = 0.365$.

iterations required the maximum computer memory available.

- The option UPWINDING was used to suppress spatial oscillations in the solutions.
- The RENUMBER command renumbered the nodes in the mesh so as to reduce the size of the global coefficient matrix.
- The starting solution for iteration was specified to be of the STOKES type.

Several grids were tested for grid independence. A comparison between the final grid chosen and one with 50% more divisions in every direction, i.e. with 3375 more elements, showed no significant difference in the flow simulations.

4.1. Numerical results: hydrodynamics

Fig. 5 shows the streamlines in the $y = 0$ plane for different fin spacing to tube diameter ratio, S. For the smallest value of S, for which $Re^* = 3.56$, the streamlines are of the Hele-Shaw type with fore-aft symmetry. This photograph can be compared with that in Schlichting [15] which is for $Re^* = 4$. As S is increased, the flow near the rear of the tube separates with the creation of a wake region with a recirculation zone. This zone becomes larger until ultimately it communicates with the region downstream and outside the fins; at this stage there is reentry of the fluid into the heat exchanger. This sequence of pictures clearly illustrates the stabilizing effect that the presence of the fin has on the hydrodynamics.

4.2. Numerical results: local heat transfer

Fig. 6 shows the distribution of Nu on the surface of the fin for different S. The pattern is similar to that found by Saboya and Sparrow [6], Fiebig et al. [11] and Valencia et al. [12]. The region of highest Nu is at the leading edge of the plate where the thermal boundary layer is thin; this, however, is not useful for heat exchanger purposes since Fiebig et al. [11] have shown that the heat flux falls sharply there on taking fin efficiency into account. For the smallest fin spacing there is no region of high Nu ahead of the tube, but as S is increased a peak appears directly in front of the tube due to the presence of a horseshoe vortex there. This

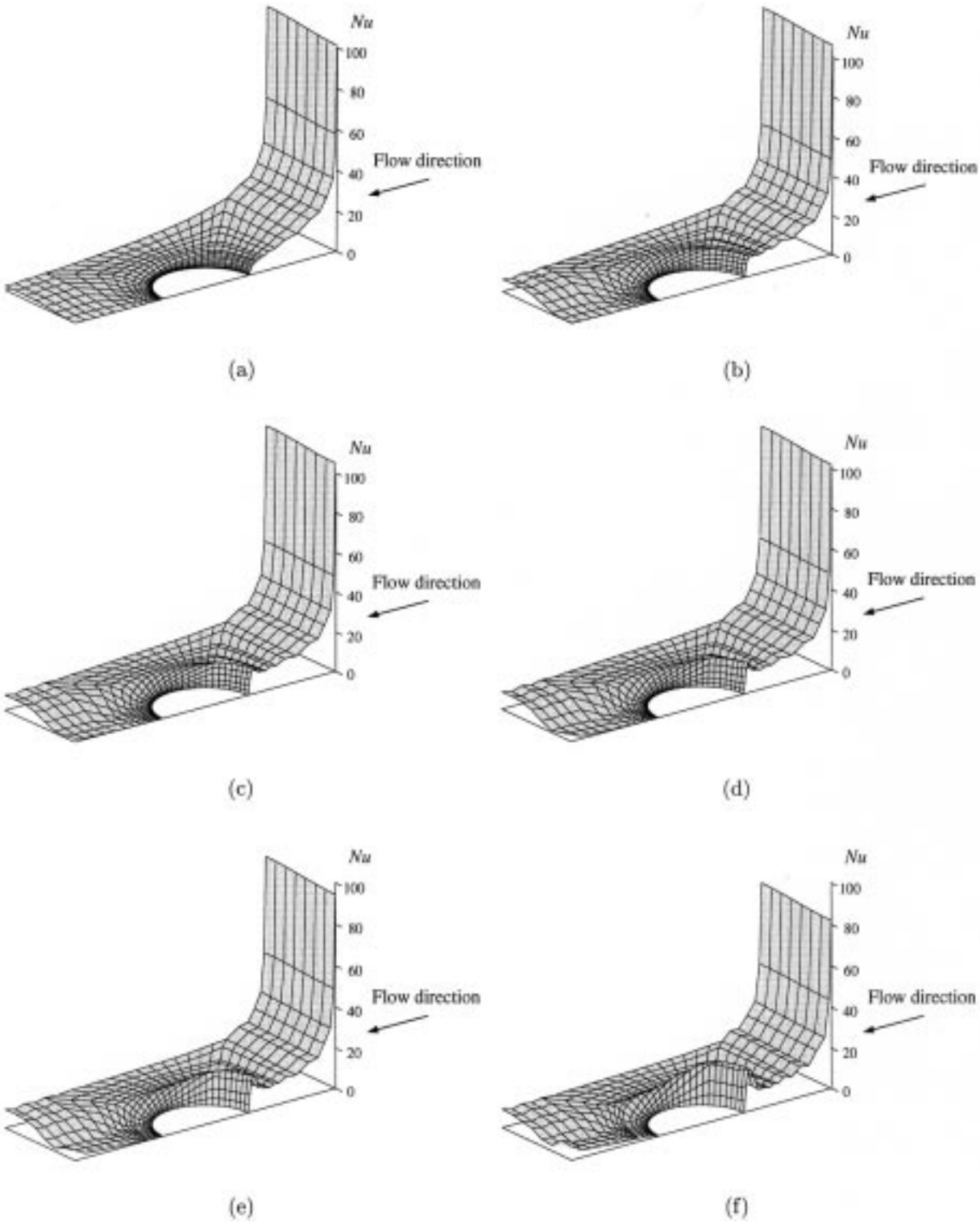

Fig. 6. *Nu* over the fin surface for $Re = 630$ and varying S. (a) $S = 0.116$, (b) $S = 0.165$, (c) $S = 0.190$, (d) $S = 0.215$, (e) $S = 0.265$, (f) $S = 0.365$.

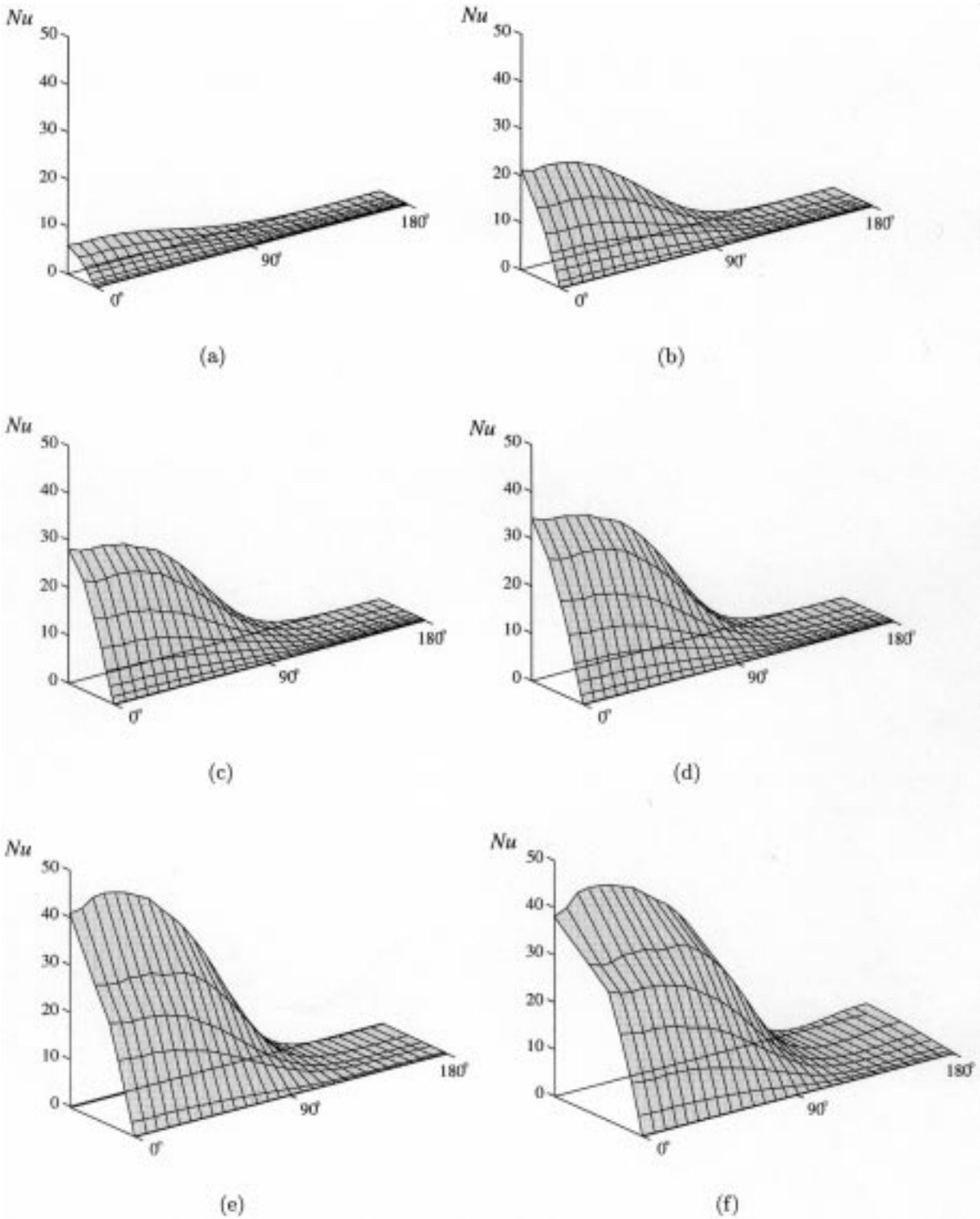

Fig. 7. *Nu* over the cylinder circumference for $Re = 630$ and varying S. (a) $S = 0.116$, (b) $S = 0.165$, (c) $S = 0.190$, (d) $S = 0.215$, (e) $S = 0.265$, (f) $S = 0.365$.

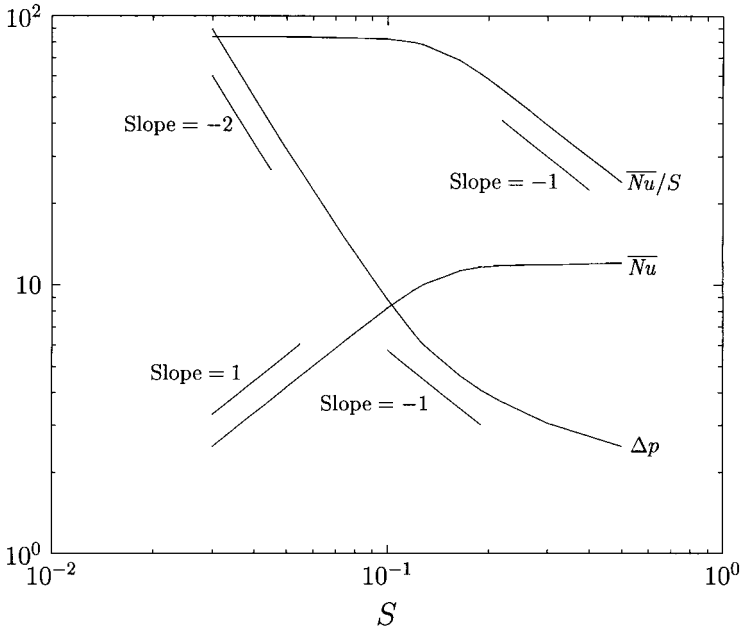

Fig. 8. $\overline{Nu}$, $\overline{Nu}/S$ and Δp vs S for $Re = 630$.

can be clearly seen in Fig. 6(f), for example. There are also significant changes in the wake region as S is increased. For the smaller values of S the fluid in the wake is essentially trapped so that Nu is very small there. As S increases and the recirculation region opens to the outside, fluid that has already left the heat exchanger reenters; this results in an improvement in the heat transfer rate in the wake region, as can be seen in Fig. 6(f). The smallest values of Nu for all S are directly behind the tube, this being a region that does not directly participate in the heat transfer.

For small S, heat transfer from the tube surface is not very important because of its small area, but becomes progressively more important as S becomes larger. Fig. 7 shows the effect that fin spacing has on the local Nusselt number around the tube. The horizontal rectangle represents the cylindrical surface of the tube, the lower edge being the fin-tube junction and the upper edge the line of symmetry. The angles are marked from the forward stagnation point. The surface of the tube can be divided into two different regions in which the Nu behavior is different: the forward-facing part up to an angle of 90° from the forward stagnation point, and the rear-facing part that is from 90° to 180°. In the forward part of the tube the Nu surface is approximately independent of angle though it grows with S; Nu is maximum at the $y = 0$ symmetry plane. Nu is much lower at the rear of the tube which does not seem to be participating in the heat transfer process.

4.3. Numerical results: overall Nusselt number

The overall Nusselt number $\overline{Nu}$, using d and $T^*_w - T^*_{in}$ as the characteristic length and temperature difference respectively, represents the heat transfer over the whole heat transfer surface, i.e. tube plus fin surface, and is one measure of the functioning of the device as a heat exchanger. From a heat balance, we can show that

$$\overline{Nu} = RePr \frac{WS}{A_f/d^2 + \pi S} \bar{T}_{exit} \tag{4}$$

where A_f/d^2 is the nondimensional fin surface, πS is the nondimensional tube surface, WS is the nondimensional flow area and $\bar{T}_{exit}$ is the average temperature at the exit section.

Fig. 8 shows several curves. One is the variation of $\overline{Nu}$ with S. As the distance between fins is increased the overall Nusselt number also increases. For small S we see that $Nu \sim S$, while for large S it becomes almost independent of S. If the interest of the heat-exchanger designer is to create a high ratio of heat transfer per unit volume of the device, the important parameter would be $\overline{Nu}/S$, which is also shown in Fig. 8, where $1/S$ is proportional to the number of fins per unit length of the tube. In addition, Fig. 8 includes the variation of pressure drop, Δp, as a function of S. Here the parameter Δp represents the difference in the nondimensional average pressure between the inlet and outlet sections of the heat exchanger. For small S, we

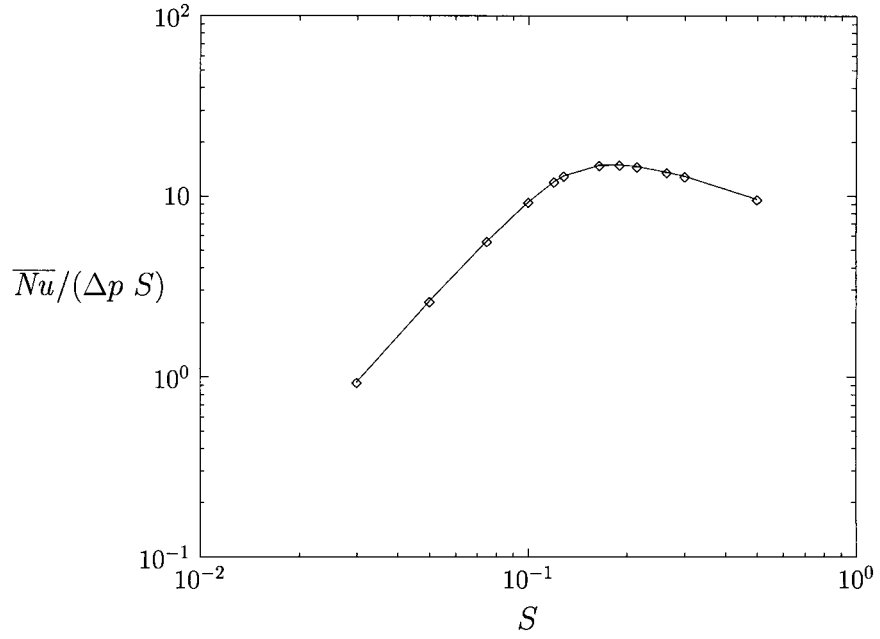

Fig. 9. $\overline{Nu}/(\Delta pS)$ vs S for $Re = 630$.

see that $\Delta p \sim S^{-2}$ while for the larger values of S it appears not to have reached an asymptote.

Some of the physics of the phenomena that go into the variation of Nu and Δp with S can be understood through simplified analyses. We will divide the discussion into three parts:

- Small S (fully developed regime): As $S \to 0$, the flow within the fins becomes fully developed hydrodynamically in a short distance from the entrance and the flow is Poiseuille-like. An expression for the pressure drop can be written as

$$\Delta p \sim \frac{L_f}{ReS^2}. \tag{5}$$

  As $S \to 0$, the fluid temperature at the exit section tends to the wall temperature. Thus, taking $\bar{T}_{exit} \to 1$ in Eq. (4), we get

$$\overline{Nu} = RePr\frac{WS}{A_f/d^2} \tag{6}$$

  indicating that $Nu \sim S$. The constant $RePrWd^2/A_f = 84.6$ in our case, which is what Nu/S in Fig. 8 tends to as $S \to 0$. In this regime the length of the tube is too short for it to be a significant factor in the heat transfer, most of which comes from the fins.
- Moderate S (combined cylinder and boundary-layers regime): In this regime the flows on each fin are independent of each other. However, the hydrodynamics and heat transfer are both affected by the presence of the tube. Let us see what we would get if we were to ignore the tube and simply assume flat-plate hydrodynamic and thermal boundary layers over each fin. Determining the pressure drop due to the acceleration of the inviscid core which comes from the growing displacement thickness of the boundary layer, we get

$$\Delta p = \frac{1}{2}\left[\left(1 - \frac{3.4L_f}{SRe^{1/2}}\right)^2 - 1\right] \approx \frac{3.4L_f^2}{SRe^{1/2}}. \tag{7}$$

From a local heat balance from the fins to the fluid, we get

$$\frac{dT}{1-T} = 0.66\frac{Pr^{4/3}}{Re^{1/2}S}\frac{dx}{x^{1/2}} \tag{8}$$

in nondimensional terms. From this the exit temperature can be determined and substituted in Eq. (4) to give

$$\overline{Nu} = RePr\frac{WS}{A_f/d^2 + \pi S} \times \left[1 - \exp\left(-\frac{1.32Pr^{4/3}L_f^{1/2}}{Re^{1/2}S}\right)\right] \tag{9}$$

As $S \to 0$, this gives $Nu \sim S$ as discussed previously for the fully developed regime. But for large S, we have

$$\overline{Nu} = 1.32\frac{Pr^{7/3}L_f^{1/2}Re^{1/2}W}{A_f/d^2 + \pi S} \quad (10)$$

The factor $A_f/\pi d^2$ is about 0.9, so that a power-law approximation cannot be obtained in the range of $S \sim O(1)$. It is important to emphasize again that in this regime there is strong influence of the tube, so that these simplifications are not strictly valid. However, neglecting the tube appears to be a better approximation for the Nusselt number than it is for the pressure drop.

- Large S (unfinned regime): It is obvious that for very large fin spacing, the hydrodynamics and heat transfer must be that around a cylinder alone; the fins will have a negligible effect, and both Δp and Nu will become independent of S. The fin spacing must be much larger than tube diameter for this to happen. We have not investigated this regime since it has been well studied by others, and also since our three-dimensional computations become time-consuming and unnecessary.

The results of Jang et al. [13] seem to be in qualitative agreement with Eqs. (5) and (6), though quantitative comparison is not possible due to differences in definition and parameter values.

The previous discussion suggests that a good design criterion may be based on $\overline{Nu}/\Delta pS$, i.e. the heat transfer per unit length of the tube per unit pressure drop, since this will take into account both compactness and pumping requirements for the heat exchanger. Fig. 9 shows how $\overline{Nu}/\Delta pS$ changes with S, the shape of the curve being dependent on the Nu and Δp variations shown in Fig. 8. It is important to note that for small S the pressure drop increases, while for large S there is a decrease in the heat transfer per unit length due to fewer fins. There is thus a maximum value of $\overline{Nu}/\Delta pS$, meaning that it is possible to obtain an optimum fin spacing under this criterion when all the other parameters are kept fixed. The optimum value of S for this Re turns out to be in the 0.128–0.240 range that the commercial heat exchanger model is sold in. The shape of the curve is also interesting in that it is seen that, if fin spacings away from the optimum are to be used, it is better to be on the side of larger fin spacing not only because it is cheaper in the sense of having less fins per unit length but also because the decrease in $\overline{Nu}/\Delta pS$ is less.

5. Conclusions

Flow visualization and numerical methods were used to study the hydrodynamics and heat convection around a cylinder between flat plates representing a single-row plate-fin and tube heat exchanger. The pair of flat plates affect each other for small spacings, and the nature of the flow strongly changes as the distance between fins is increased. Upstream of the tube there is no vortex system at first as the systems due to the two fins cancel themselves out. The vortices show up as the fin spacing is further increased. The region downstream of the tube is dominated by the wake. For small fin spacings, the flow is of the Hele-Shaw type with fore-aft symmetry. As the spacing increases, a separation zone is formed behind the cylinder. This is closed at first but then opens up to the downstream fluid.

The hydrodynamics determine the heat transfer and the distribution of the local Nusselt number. On the fin, it is highest at the leading edge due to the thin boundary layer, and at the front of the tube when a horseshoe vortex system is present there. Heat transfer in the wake is slightly increased once the recirculation region opens to the trailing edge and reentrant fluid comes in. The front of the tube also participates more in the heat transfer process than does the back. The fin spacing very strongly influences the overall Nusselt number and the pressure drop. If the overall Nusselt number per unit length per unit pressure drop is used as a criterion, there is an optimum with respect to fin spacing. If it is too small, the pressure drop is high; if it is too large, there are too few fins for effective heat transfer.

Though this study has been with respect to fin spacing, the effect of Reynolds number was also studied experimentally and numerically. The trend with respect to increasing Re was found to be similar to that of increasing S, i.e. Hele-Shaw flow at low Re, wake with closed recirculation region at higher Re, then a wake with a separation region open to the downstream fluid, and finally oscillations in the wake. Thus there appears to be a range where ReS is the parameter that determines the flow. Of course, ReS^2 is the parameter for Hele-Shaw flow and Re itself for large S where the fins do not have any significant influence on the flow.

Although the investigation here has been for single-row heat exchangers, many of the conclusions also apply to multi-row devices. The latter are in fact more dependent on fin spacing since the entrance region with high heat transfer rates is only present in the first row. The following rows depend much more on the high heat transfer regions around the cylinders which, as we have shown, are very dependent on fin spacing.

Acknowledgements

We thank CONACyT for a Fulbright Fellowship for R.R.-M. and BRGD-TNDR for support of this research.

References

[1] H.S. Hele-Shaw, Investigation of the nature of surface resistance of water and of stream motion under certain experimental conditions, Proc. Roy. Inst. 16 (1899) 49.

[2] M. Coutanceau, J.R. DeFaye, Circular cylinder wake configurations: a flow visualization survey, Applied Mechanics Reviews 44 (1991) 255–305.

[3] C.J. Baker, The laminar horseshoe vortex, Journal of Fluid Mechanics 95 (1979) 347–367.

[4] C.J. Baker, Oscillations of horseshoe vortex systems, ASME Journal of Fluids Engineering 113 (1991) 489–495.

[5] U. Bossel, F.V. Honnold, On the formation of horseshoe vortices in plate fin heat exchangers, Archives of Mechanics 28 (1976) 773–780.

[6] F.E.M. Saboya, E.M. Sparrow, Local and average transfer coefficients for one-row plate fin and tube heat exchanger configurations, ASME Journal of Heat Transfer 96 (1974) 265–272.

[7] P.T. Ireland, T.V. Jones, Detailed measurements of heat transfer on and around a pedestal in fully developed passage flow, in: Proceedings of the Eighth International Heat Transfer Conference 3, 1986, pp. 975–980.

[8] A. Haught, M.S. Engelmann, Numerical and experimental simulation for airflow and heating in a tube fin heat exchanger, Heat Transfer in Gas Turbine Engines and Three-Dimensional Flows HTD-103 (1988) 107–113.

[9] K. Torikoshi, G. Xi, Y. Nakazawa, H. Asano, Flow and heat transfer performance of a plate-fin and tube heat exchanger, first report: effect of fin pitch, in: Proceedings of the Tenth International Heat Transfer Conference, 1994, pp. 411–416.

[10] A. Bastani, M. Fiebig, N.K. Mitra, Numerical studies of a compact fin-tube heat exchanger, in: W. Roetzel, P.J. Heggs, D. Butterworth (Eds.), Design and Operation of Heat Exchangers, Springer-Verlag, Berlin, 1992, pp. 154–163.

[11] M. Fiebig, A. Grosse-Gorgemann, Y. Chen, N.K. Mitra, Conjugate heat transfer of a finned tube Part A: heat transfer behavior and occurrence of heat transfer reversal, Numerical Heat Transfer, Part A 28 (1995) 133–146.

[12] A. Valencia, M. Fiebig, N.K. Mitra, Heat transfer enhancement by longitudinal vortices in a fin-tube heat exchanger element with flat tubes, ASME Journal of Heat Transfer 118 (1996) 209–211.

[13] J.-Y. Jang, M.-C. Wu, W.-J. Chang, Numerical and experimental studies of three-dimensional plate-fin and tube heat exchangers, International Journal of Heat and Mass Transfer 39 (1996) 3057–3066.

[14] R. Romero-Méndez, Study of external heat transfer mechanisms in single-row fin and tube heat exchangers, Ph.D. dissertation, Department of Aerospace and Mechanical Engineering, University of Notre Dame, Notre Dame, IN 46556, USA, 1998.

[15] H. Schlichting, Boundary-Layer Theory, McGraw-Hill, New York, 1968.